Remarkable hydrogen storage properties of MgH2doped with VNbO5

Remarkably Hydrogen Storage Properties of MgH_2 doped by $VNbO_5$

Antonio Valentoni[1*], Gabriele Mulas[1], Stefano Enzo[1], Sebastiano Garroni[2,3]

[1]Department of Chemistry and Pharmacy, Università degli Studi di Sassari e INSTM, Via Vienna 2, I-07100 Sassari Italy.

[2]International Research Centre in Critical Raw Materials-ICCRAM, University of Burgos, Plaza Misael Banuelos s/n, 09001 Burgos, Spain

[3]Advanced Materials, Nuclear Technology and Applied Bio/Nanotechnology. Consolidated Research Unit UIC-154. Castilla y Leon. Spain. University of Burgos. Hospital del Rey s/n, 09001 Burgos, Spain

* Corresponding authors: Antonio Valentoni

E-mail address (corresponding author): avalentoni@uniss.it

E-mail address (co-authors): mulas@uniss.it, enzo@uniss.it, sgarroni@ubu.es

ABSTRACT

The present work concerns the catalytic effect of $VNbO_5$, a ternary oxide prepared by solid-state route, on the sorption performance of MgH_2. Three doped systems, namely 5, 10 and 15 wt. % $VNbO_5$-MgH_2 have been prepared by ball milling and thoroughly characterized. Hydrogen sorption, evaluated by temperature programmed desorption experiments, revealed a significant reduction of the desorption temperature from 330 °C for the un-doped sample (prepared and tested for comparison) to 235 °C for the $VNbO_5$-doped sample. Furthermore, more than 5 wt. % of hydrogen can be absorbed in 5 minutes at 160 °C under 20 bar of hydrogen, which is remarkable compared to the 0.7 wt. % achieved for the un-doped system. The sample doped with 15 wt.% of additive, showed a good reversibility: over 5 wt. % of hydrogen with a negligible degradation even after 70 consecutive cycles at 275 °C and 50 cycles at 300 °C. The kinetics analysis carried out by the Kissinger's method exhibited a considerable reduction of the activation energy for the desorption process. Finally, Pressure-Composition-Isotherm experiments conducted at three different temperatures allowed to estimate the thermodynamic stability of the system and shed light on the additive role of $VNbO_5$.

KEYWORDS: Solid state hydrogen storage; Magnesium hydride; Vanadium Niobium Oxide; Kinetic and Thermodynamic

1 INTRODUCTION

The use of hydrogen as carbon-free energy vector is one of the most suitable technological challenges for mitigating the carbon dioxide emissions caused by the extensive exploitation of the carbon fossil fuels.[1] The commercialization of the hydrogen fuel cell vehicles (FCVs) represents, for example, a "greener" and efficient alternative to the gasoline internal combustion engine ICE responsible for 17 % of total CO_2 emission in EU (2008). However, in order to promote a rapid diffusion of this technology into the global market, obstacles related to the storage and the transport of hydrogen have to be overcome. The most exploited solutions such as hydrogen liquid and high-pressure tank, suffer of high costs and safety constrains which limit their exercise in several countries.[2]

Based on these considerations the search of an efficient, safe and less expensive hydrogen storage approach is becoming of primary importance. Solid-state hydrogen storage presents potential advantages in terms of volumetric density and safety compared to the pressurized gas technology.[3] In this framework, vast numbers of materials have been investigated in order to find a valid candidate able to ab/de-sorb reversibly hydrogen at moderate temperatures, satisfying the DOE requirements.[4-6] Among them, MgH_2 system remains one of the most studied and interesting compound for solid-state hydrogen storage, due to its high gravimetric capacity of 7.6 wt. % combined with relative cheap cost (< 3 €/kg) and abundance (7^{th} element in the earth).[7] However, it presents several limitations for practical application, for example a very high desorption temperature of 400-450 °C and slow kinetics at temperatures below 400 °C.[8, 9] Various strategies have been proposed in order to improve the hydrogen sorption properties of MgH_2, and, among them, the combination with other complex hydrides[10-14] and the doping with metals,[15-18] metals halides[19-21] and metal oxides,[22-26] probably represent the most performing approaches reported in the current literature.

The addition of metal oxides, in particular, produced a clear benefit in terms of hydrogen sorption kinetics and desorption temperature. Since the pioneering work of Barkhordarian et al. [22] which demonstrated the extraordinary catalytic effect of Nb_2O_5 on the MgH_2 sorption performance, many attentions have been addressed to this additive.[22-26] To get insight into the catalytic mechanism, in situ experiments have evidenced the crucial role played by the Mg-Nb oxide phases formed during the sorption reaction of the Nb_2O_5-doped MgH_2 system.[27] This ternary oxide, conversely to MgO, facilitate the diffusion of hydrogen into the Mg bulk and assists the hydrogen splitting reaction, then improving the sorption properties of the whole system.[28] Friedrichs et al. demonstrated that the Mg-

Nb-oxide limits the grain growth of Mg during desorption preserving the grain boundaries for the hydrogen diffusion. Further studies conducted by TEM, XPS and EDX, showed that during the mechanical treatment, the nanosized Nb oxide diffuses into the MgH_2 matrix and starts a reducing process of the Nb oxide.[29, 30] During the heating treatment, Nb in the high valence state (V) was further reduced by Mg, forming various mixed Mg-Nb oxide compounds. The ability to easily change the oxidation number during the de/hydrogenation cycles, and the high accessible valence state, facilitate the hydrogen transport into the Mg matrix reducing the kinetics barriers.[29, 30] Among the Mg-Nb oxides families, only $Mg_3Nb_6O_{11}$ presented a reversible interaction with H_2.[31] This was ascribable to the crystal structure of the compound, characterized by the presence of Niobium octahedral clusters inside the oxide lattice, different than the other Mg-Nb oxides investigated.[31]

From this specific literature, it emerges that the Nb-octahedral coordination geometry could play a key role to improve the hydrogen sorption properties of Mg-based systems. Similar microstructure properties were also satisfied in vanadium-doped Mg compounds with enhanced hydrogen storage properties.[32-34] However, despite the several numbers of additives tested, no data are reported in the current literature, by our knowledge, concerning a synergic effect of the V-Nb oxide phase characterized by octahedral clusters. A restricted number of stoichiometric and non-stoichiometric V-Nb-O compounds with different composition have been studied sporadically, and their crystal structure were not always determined unquestionably. Among them, only the $VNbO_5$ compound meets the local octahedral coordination.[35-38]

Based on these considerations, the present investigation provides, for the first time, a detailed study of the effect of $VNbO_5$ on the sorption properties of magnesium hydride. The additive, prepared by conventional route, is able to improve significantly the sorption properties of the system decreasing the desorption temperature and enhancing the cyclability of the whole system. Experimental methods are described in the following.

EXPERIMENTAL

Commercial powders of MgH_2 (hydrogen storage grade) were purchased from Sigma Aldrich, while crystalline $VNbO_5$ was prepared by a prolonged annealing at 500 °C (2 h) of the pre-milled powders (200 h) containing a mixture of V_2O_5 (99%) and Nb_2O_5 (99%) in a molar ratio 1:1. The MgH_2-xwt% $VNbO_5$ (x = 0, 5, 10, 15) samples were then prepared by ball milling. For each system, 8 grams of powders were ball milled for 10 hours in a stainless steel vial with 2 balls (8 grams each one).

All the mechanical treatments have been performed using a Spex/Mixer mill model 8000 working at 875 rpm and under inert atmosphere of Ar. Manipulation of the samples was performed inside a glove box MBraun with O_2 and H_2O levels < 1 ppm.

The sorption properties of the samples were investigated by temperature programmed desorption experiment (TPD) using a Sievert-based instrument Setaram PCT-Pro 2000 (pressure accuracy 1%). The composite was heated from room temperature to 400 °C at 5 °C/min followed by an isothermal treatment of 2 h. A second desorption via heating up to 300 °C was carried out with the same modalities. All experiments were carried out under static vacuum. The absorption performance was evaluated at 160 °C after submitting the sample to 20 bar of pure hydrogen for 3 h. After that, the sample was cooled to room temperature while maintaining a back pressure of 20 bar to prevent any desorption process. The life cycle experiment was performed after two activation dis-charging cycles: the dehydrogenated sample was measured at 250 °C, 275 °C and 300 °C under static vacuum, while 20 bar of hydrogen was applied for the absorption step. The Pressure-Composition-Isotherm (PCI) experiments were conducted after the cycle life experiment previously described. The measurement was carried out at 3 different temperature of 275 °C, 300 °C and 325 °C, with pressures of 0-15 bar for the absorption, and 15-0 bar for the desorption steps. All measurements were conducted in Δp mode, using an increasing pressure of 1.5 bar per step (dwell time 90 min).

Calorimetric measurements were performed on the as-milled powders by using a Sensys DSC Setaram. The sample holder was charged with ~50 mg of powder under Ar atmosphere (1 bar) and the experiment conducted from room temperature to 500 °C. Five increasing heating rates were selected for the experiments, namely: 2 °C/min; 5 °C/min; 10 °C/min; 15 °C/min and 20 °C/min.

Structural and microstructural characterization have been performed by X-ray powder diffraction technique, using a Rigaku Smart Lab with a Bragg–Brentano geometry using Cu Kα radiation (1.54178 Å) and a monochromator in the diffracted beam. For each analysis 0.3 grams of powders, stored in the glove box, were placed in an air-sensitive sample holder covered by an airtight hood of Kapton foil to prevent contact with air moisture and oxygen during the analysis. The microstructural parameters were then evaluated by fitting the XRPD patterns by means the MAUD, a Rietveld refinement software.[39]

RESULTS AND DISCUSSION

Sorption and Structural properties

The synthesis of $VNbO_5$ was successfully demonstrated by *ex situ* X-ray diffraction and reported in Figure 1 together with the patterns of the un-milled (0 h) and milled (200 h) systems. The starting reagents were represented by the monoclinic Nb_2O_5 (ICSD 01-071-0005), space group *P2/m*, and

orthorhombic V_2O_5 (ICSD 01-072-0433) space group *Pmnm*. The XRD pattern of the composite after long milling treatment (200 h) was totally different, with the disappearance of the initial oxides and the presence of an amorphous phase together with the orthorhombic $Nb_{16.8}O_{42}$ (ICSD 01-071-0336) phase. After the thermal treatment at 500° C, peaks ascribable to the crystalline $VNbO_5$ (ICSD 00-046-0046) were observed together with $Nb_{16.8}O_{42}$ in trace (<5 wt.%). The XRD pattern of $VNbO_5$ obtained by the solid-state route can be unambiguously identified and compared with previous data reported in the literature.[38]

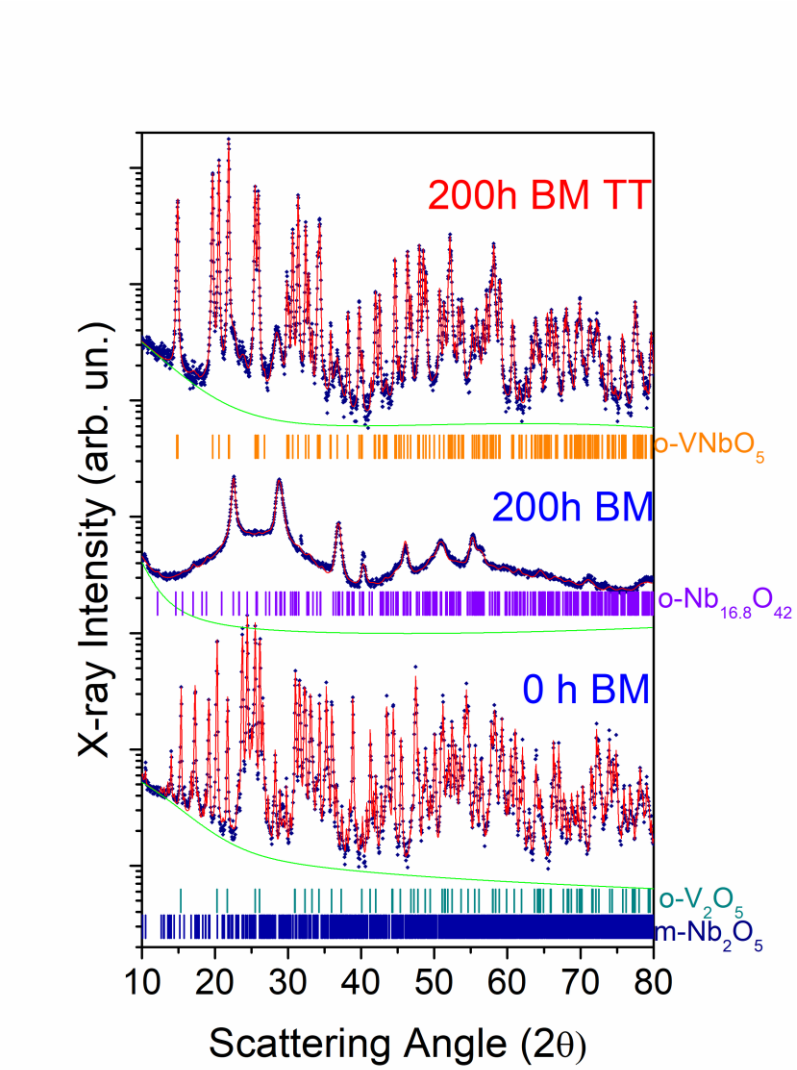

Figure 1. XRD patterns and the correspond interpolations of the equimolar mixture V_2O_5 and Nb_2O_5 un-milled (0h BM, Rwp % 7.4), 200 h ball milled (200h BM, Rwp % 4.2) and of the as-milled sample after the thermal treatment at 500 °C (200h BM TT, Rwp % 5.6). In the bottom are reported the ticks of the crystalline phases present in the patterns. The experimental patterns, best fit profiles and the backgrounds are represented by blue squares, red and green line, respectively.

.

Three different batch of pristine MgH_2 were then ball milled for 10 hours with increasing amount of $VNbO_5$, namely, 5 wt.%, 10 wt.% and 15 wt.%. In order to evaluate the effect of $VNbO_5$, temperature programmed desorption (TPD) measurements of the samples were recorded and compared in Figure 2. The TPD profiles reported in Figure 2a, revealed similar dehydrogenation behavior, with all the samples releasing hydrogen in a single step. On the other hand, the onset desorption temperatures of the doped and un-doped composites, decreased simultaneously with the increasing of $VNbO_5$ amount. Un-doped MgH_2 started to release hydrogen at around 330 °C, with a total amount of 6.67 wt.% reached at 400 °C, lower than the theoretical gravimetric capacity expected (7.6 wt.%). This reduction was probably ascribable to the presence of MgO impurities in the starting material and to the partial hydrogen release induced by the high-energy ball milling during the preparation. Compared to the un-milled MgH_2, the onset temperature was decreased by 100 °C in agreement with previous studies.[40] When MgH_2 was milled with 5 wt. % of $VNbO_5$, the temperature release of hydrogen further decreased to 270 °C with a total dehydrogenation of 6.27 wt. % H_2 at 400 °C. For the samples doped with 10 wt.% and 15 wt.% of $VNbO_5$, the onset desorption temperatures were reduced to 264 °C (6.07 wt. % - 400 °C) and 234 °C (5.89 wt.% - 400°C), respectively. The total amount of hydrogen evolved for these doped systems, at 400°C, was lower if compared with the un-doped MgH_2. However, considering their theoretical capacity, they desorbed the 86 (5 wt.%), 87 (10 wt.%) and 89 % (15 wt.%).

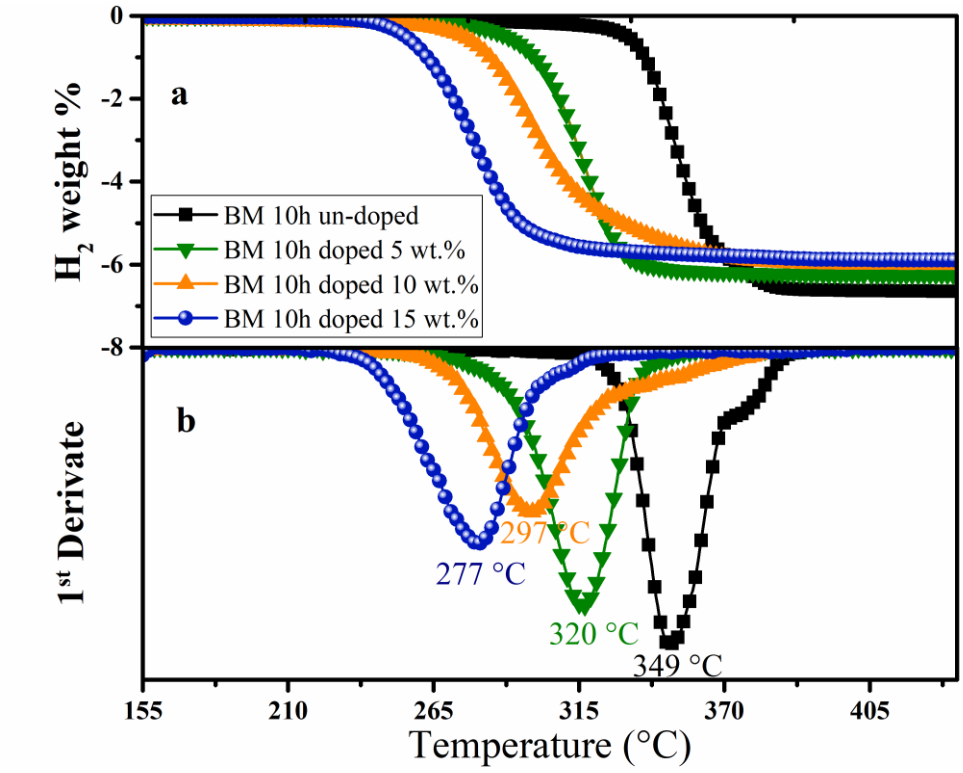

Figure 2. **a**) Temperature programmed desorption (TPD) profiles of the un-doped MgH_2 milled 10 h (dark squares) and of the MgH_2 systems milled (10h) with 5 wt.% (olive triangles), 10 wt.% (orange triangles) and 15 wt.% (blue circles) $VNbO_5$. **b**) 1st derivate of the TPD measurements reported in the panel a.

In order to better evaluate the different TPD results, the 1st derivative of the desorption profiles were calculated and reported in Figure 2b. The inspection of the first derivative allowed to determine the maximum desorption peak and helped to distinguish multiple desorption processes when they occur consecutively and/or very close. The graph confirmed the trend observed for the integral desorption curves, with a reduction of the onset desorption temperatures when the additive content was increased. The same trend was observed for the hydrogen desorption peak maxima. In fact, the un-doped MgH_2 sample started to release hydrogen at 330 °C, with a peak maximum centred at 349 °C. For the 5 wt. %, 10 wt. % and 15 wt. % doped samples, the peak temperatures of 320 °C, 297 °C and 277 °C were observed. The latter result is quite interesting because the dehydrogenation step occurred in a range between 230 °C - 300 °C. Note that, at these temperatures, pristine MgH_2 is quite stable, suggesting a large destabilization due to the presence of $VNbO_5$. This insight appears of major interest if compared with the results obtained by the addition of other transition metals mixed oxides. For example, the addition of $CoFe_2O_4$, $ZnFe_2O_4$, $MnFe_2O_4$ and $Mn_{0.5}Zn_{0.5}Fe_2O_4$ nanoparticles on MgH_2, improved significantly the sorption kinetics only at temperatures higher than 300 °C, with the maximum peaks located around 330 °C - 350 °C.[41]

The de-hydrogenated composites doped with 10 wt.% and 15 wt.% of $VNbO_5$ were re-hydrogenated and then subjected to a new heating ramp from room temperature to 300 °C. In Figure 3a, the second desorption cycle versus the heating temperature, is reported. The onset temperature of 200°C was observed for the both doped samples, with a decrease of 60 °C (15 wt.%) and 30 °C (10 wt.%), if compared to the first step. Additionally, hydrogen gas was completely released at 285 °C.

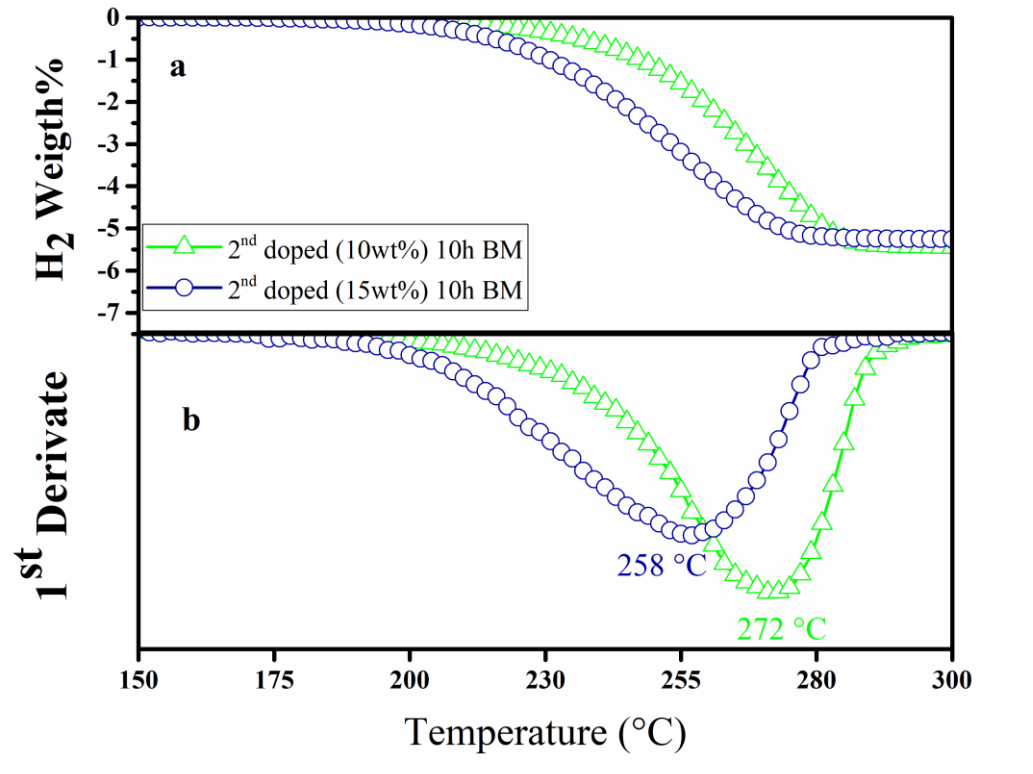

Figure 3. **a)** 2nd TPD profiles of MgH_2 doped with 10 wt.% (green triangles) and 15 wt.% (blue circles) of $VNbO_5$. **b)** 1st derivate of the TPD measurements reported in the panel **a**.

The derivative plot, depicted in Figure 3b, confirmed the data observed in the previous analysis. Focusing on the hydrogen storage properties, the sample doped with 15 wt.% of $VNbO_5$ released 50 % of hydrogen at 250 °C and the 99 % at 275 °C. As clearly emerged in Figure 4, the second desorption event of the 10 wt.%-doped sample was lower compared to the 15 wt.% sample, but significantly higher with respect to first desorption in the whole range of the temperatures analysed. This also confirmed the beneficial effect of the activation process in the composites, although further structural investigations are necessary to confirm this point."

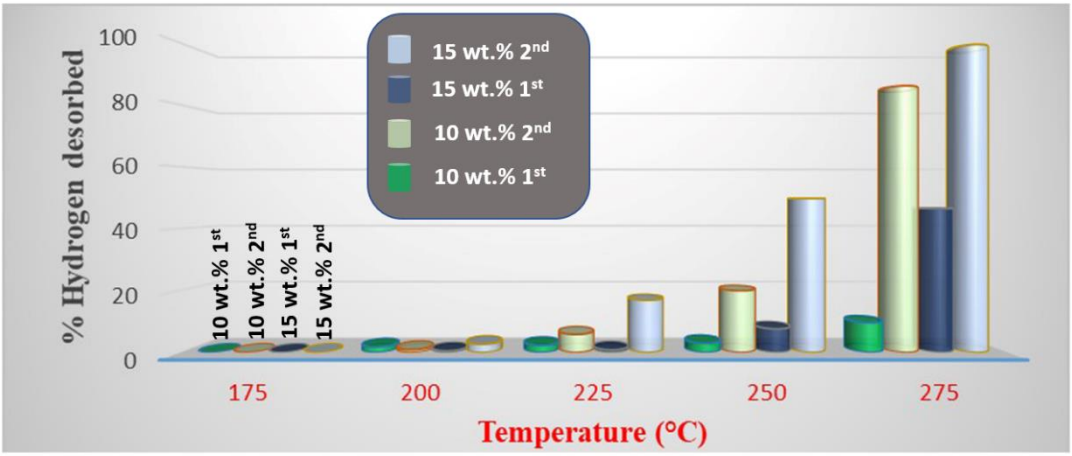

Figure 4. Percentage of the total hydrogen released during the first and second desorption step of the MgH_2 doped with 10 and 15 wt.% of $VNbO_5$, as a function of the temperatures ramp. The green (1^{st} des step) and light green (2^{nd} des step) cylinders are referred to the 10 wt.% doped sample, whereas the dark blue (1^{st} des step) and sky blue (2^{nd} des step) cylinders are referred to the15 wt.% doped sample. The percentage values have been calculated starting from the total amount of hydrogen evolved experimentally for each sample.

Concerning the absorption analysis, reported in Figure 5a, the systems with 5 wt. %, 10 wt. % and 15 wt. % of $VNbO_5$ stored a maximum of 4.60, 5.58 and 5.34 wt. % of hydrogen, after 60 minutes. This is a significant improvement if compared with the un-doped MgH_2 system able to re-adsorb only 1.5 wt. % of hydrogen after 60 minutes. However, different sorption kinetics were evidenced during the first 30 minutes; in particular the samples doped with 10 wt. % and 15 wt. % of $VNbO_5$ absorbed more than the 5 wt. % of hydrogen, higher with respect to the 4.4 wt. % H_2 observed in the 5 wt.%-doped samples.

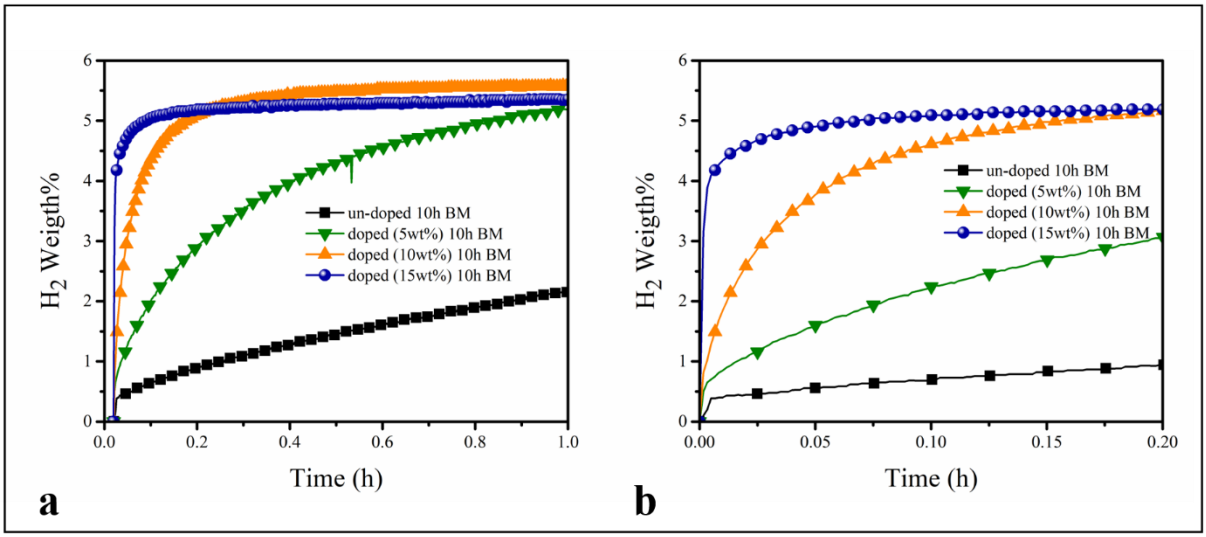

Figure 5. **a**. Absorption profiles recorded at 160 °C and 20 bar of H_2 on the un-doped and doped MgH_2. **b.** Zoom panel of the absorption profile in the first 10 minutes.

The sample with 15 wt. % of additive, confirmed the best performance observed in the desorption investigation (see Figure 5b): 50 % of the total hydrogen was absorbed just in 1.25 minutes while 5 minutes were required to reach the 90 % of the theoretical amount under moderate conditions of 160°C and 20 bar of H_2. For comparison, the sample with 10 wt.% of $VNbO_5$, absorbed the 15 and 72 % after 1.25 and 5 minutes, respectively.

Based on these promising results, the investigation was then focused on the MgH_2 doped with 15 wt.% of $VNbO_5$ in order to evaluate its performance for several ab-desorption cycles (50). The amount of H_2 (wt. %) charged and dis-charged versus the cycle number is shown in Figure 6 for three different working temperatures (250 °C, 275 °C and 300 °C). At 300 °C (red squares in Figure 6a), the sample stored reversibly over 5-5.5 wt. % of H_2 for 50 cycles.

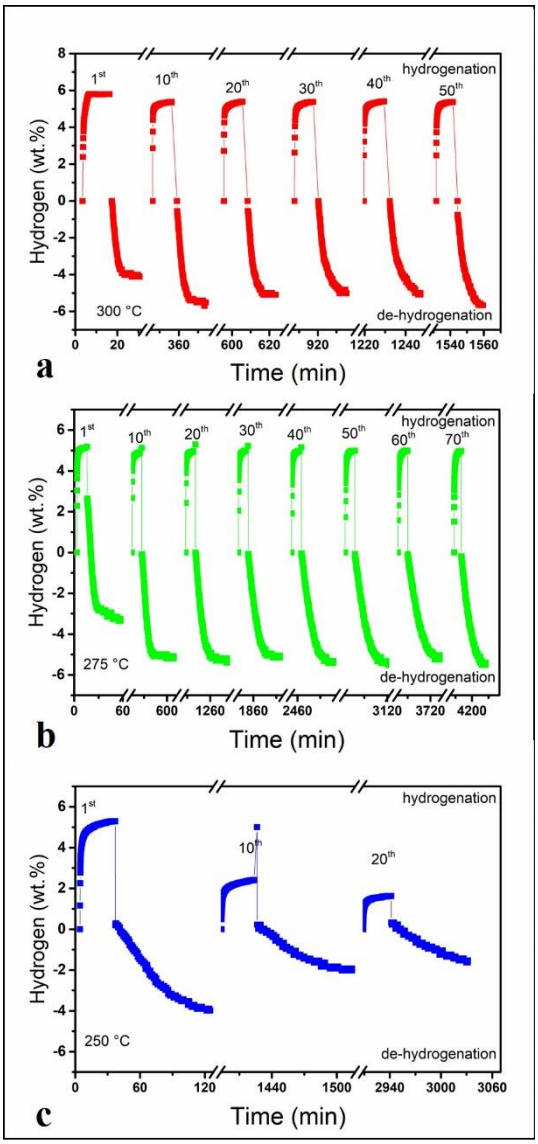

Figure 6. Amount of hydrogen (wt. %) ab-desorbed in the MgH_2 doped with 15 wt% of $VNbO_5$ as a function of the cycle number performed at 300 °C (panel **a**), 275 °C (panel **b**) and 250 °C (panel **c**). The desorption was carried out under static vacuum (45 minutes) and the absorption under 20 bar of H_2 (10 minutes).

At lower temperature of 275 °C (green squares in Figure 6b), the system stored reversibly a significant amount of 5-5.25 wt.% H_2 for 72 cycles. This result indicated the high stability of the composite in these operative conditions. On the other hand, at 250 °C (blue squares in Figure 6c), after the 10^{th} cycle, the system ab/desorbed only the 3 wt. % of hydrogen and below the 2 wt.% upon the 20^{th} cycle.

To integrate the results obtained during the cyclability experiments on the 15 wt.% -doped system, the hydrogen rate values achieved at 300 °C were reported in Table 1 and compared to those obtained in similar conditions for other highly-performing magnesium-catalysed systems presented in the recent literature.[25, 42-45]

Additive	*Desorption at 300 °C (wt% H_2 min^{-1})*	*Absorption at 300 °C (wt% H_2 min^{-1})*
$VNbO_5$	**1.49**	**3.46**
Ni[42]	0.03	1.86
V[42]	1.66	-
Cr_2O_3[43]	0.07	1.17
$MnFe_2O_4$[44]	0.08	-
Nb_2O_5 [45]	2.50	3.00
Nb_2O_5+Cr_2O_5[25]	0.25	1.20

Table 1. Hydrogen kinetic rate values (wt. % H_2 min^{-1}) of several catalysed MgH_2 systems obtained for the desorption and absorption steps under 300 °C.

As clearly emerged from the data reported in Table 1, the kinetics rates achieved with the addition of $VNbO_5$ were significantly higher than those obtained in the $MnFe_2O_4$-, Cr_2O_3-, Ni- and Nb_2O_5/Cr_2O_5- based systems. Furthermore, a substantial enhancement could be also observed with respect to the Nb_2O_5- and V-catalysed systems for both the hydrogenation steps, supporting a synergetic effect when the two compounds are combined.

With the aim to investigate the crystalline phases in the 15 wt.%-doped system during the cycling experiments conducted under 275 °C, X-ray diffraction patterns were acquired on the crystalline powders after the desorption and absorption steps, and compared with the as-milled mixture. As shown in Figure 7, in the initial system, the ball milling promoted a partial conversion of β-MgH_2 (<*D*> 140 ± 5 Å) in the γ-MgH_2 (<*D*> 180 ± 5 Å) polymorph. Furthermore, the presence of nanocrystalline MgO (< 5 wt.%) was also observed. No peaks ascribable to Nb- or V- related phases

were detected in the initial pattern. $VNbO_5$ reflections could not be observed due to the nanostructuring process induced by the mechanical treatment. The XRD analysis on the powders upon the desorption (275 °C) revealed the presence of 91 wt.% of Mg metallic (<*D*> 1100 ± 10 Å) together with 7 wt.% of nanocrystalline MgO (<*D*> 90 ± 5 Å). The peaks related to the γ-MgH_2 completely disappeared while traces of β-MgH_2 (< 2 wt.%) could be still detectable. This was apparently in contrast with the plateau reached in the volumetric measurements for the catalysed-systems. However, the H_2 evolved upon the desorption step in the reactor, was probably enough to react with the dehydrogenated powders before being evacuated at room temperature for the XRD measurements. Concerning MgO, its presence could be explained by the long-time collection (12 h) of the patterns necessary for achieving a reasonable pattern suitable for the Rietveld refinement. Furthermore, a contribution from the $VNbO_5$ can not be excluded although no evidence of crystalline V- or Nb- or related phases were visible in the diffraction pattern. It is also important to highlight that the amount of MgO extrapolated from the quantitative analysis was in line with the experimental measurements of the hydrogen evolved and its strong peaks emerged because log*q scale has been used for the intensity, emphasizing smaller reflections. Similar conclusions could be also made for the pattern collected on the powders after re-absorption (275 °C) and visualized in Figure 7. β-MgH_2 (<*D*> 900 ± 10 Å) was the main phase observed in the final pattern (90 wt.%) with trace of unreacted Mg (< 3 wt.%) and MgO (< 7 wt.%).

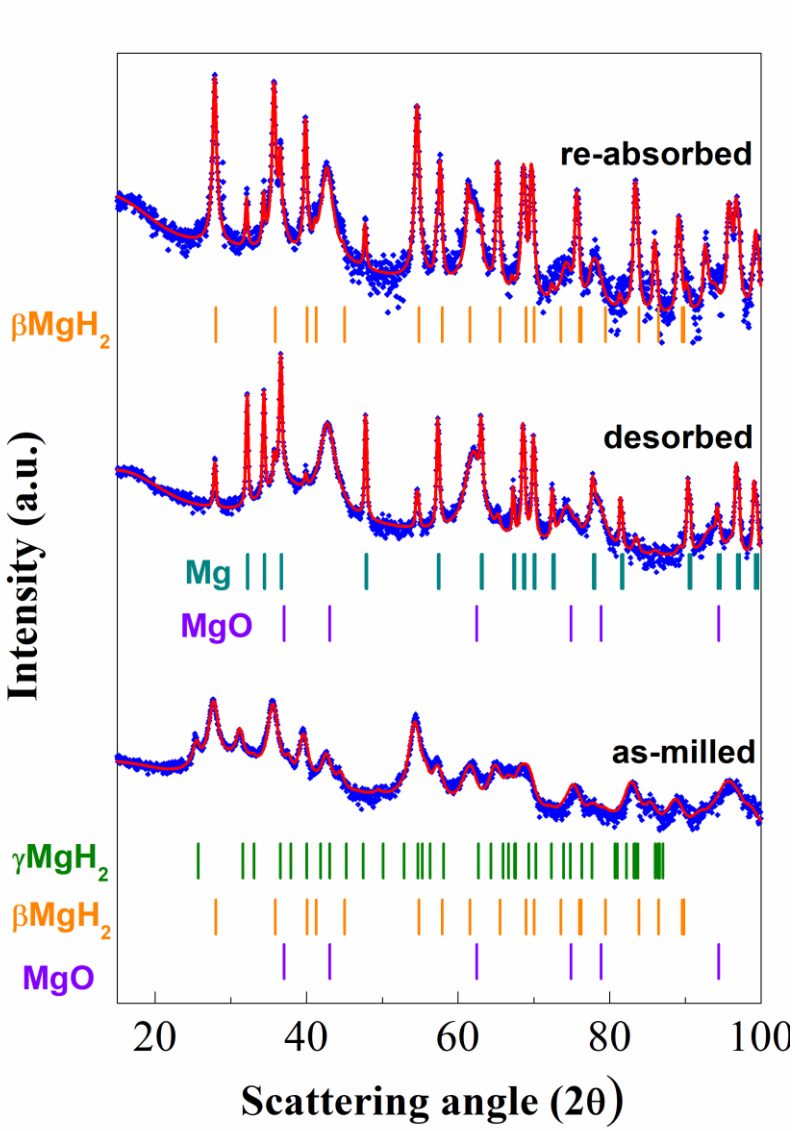

Figure 7. Experimental (blue squares) and Rietveld refined (red solid line) XRD patterns of the 15 wt.%-doped MgH_2 after the desorption and absorption step (5th cycle). XRD pattern of the as-milled system is also showed for comparison.

Kinetics and thermodynamic investigations

The analysis of the microstructure parameters of the patterns reported in Figure 7, evidenced that after cycling the crystallite dimensions of the β-MgH_2 phase increased significantly while the hydrogen storage performances of the whole system were preserved (see Figure 6). That means that the initial nanostructured conditions of the system did not influence the performance of the MgH_2-15wt.% $VNbO_5$ sample. In other words, the activity of the $VNbO_5$ additive should play a central role for enhancing the hydrogen storage properties of MgH_2. Based on this consideration, in order to better

evaluate the effect of the additive, the activation energy of the 15 wt%-doped system, has been evaluated by the Kissinger method using the following equation:[46]

$$\frac{d\ln(\frac{\beta}{T_m^2})}{d(\frac{1}{T_m})} = -\frac{E_a}{R} \qquad \text{eq. 1}$$

where β corresponds to the heating rate, T_m the peak temperature and R the gas constant.

DSC profiles, reported in Figure 8, have been acquired for the un-doped (panel **a**) and doped system (panel **b**), varying the heating rate (2, 5, 10, 15 and 20 °C). As expected, the endothermic peaks corresponding to the maximum rate of dehydrogenation shifted to higher temperatures as the heating rate was increased for both the samples.

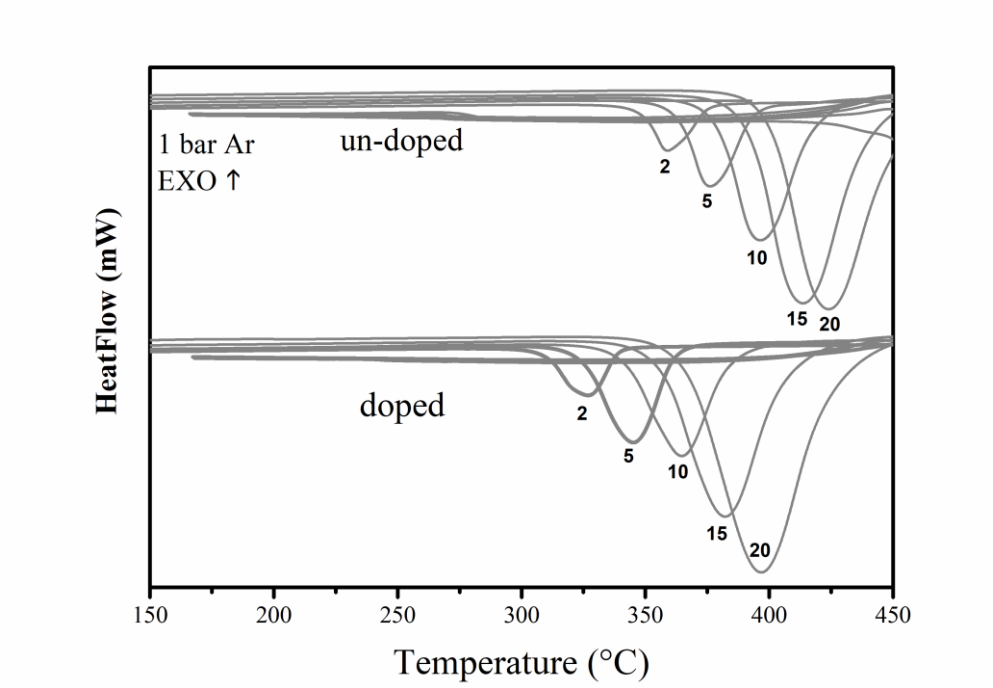

Figure 8. DSC curves of the un-doped (panel a) and doped (panel b) MgH_2 recorded at different heating ramps of 2 °C/min; 5 °C/min, 10 °C/min, 15 °C/min and 20 °C/min.

For all the heating rates, the hydrogen release onsets and peaks maximum started at lower temperatures for the doped systems, corroborating the previous results obtained by the manometric apparatus. The discrepancy temperatures with respect to the TPD experiments (static vacuum), were due to the different pressure conditions used in the DSC analysis (1 bar Ar). The plot based on the Kissinger equation (eq. 1), is shown in Figure 9.

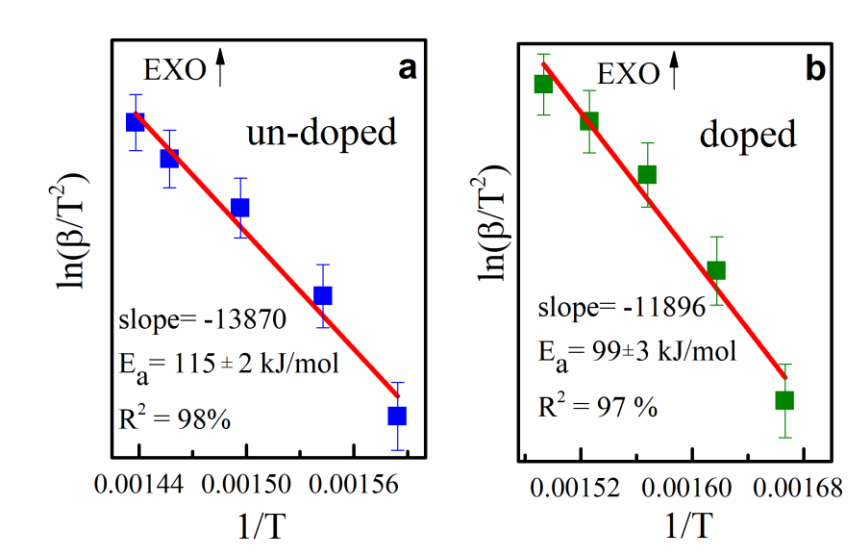

Figure 9. Kissinger plots and the related Activation Energy (E_a) values of the un-doped and 15 wt. $VNbO_5$-doped MgH_2.

A good linear relationship between $\ln(\beta/T^2_{max})$ and $1/T_{max}$ was obtained for all the samples, allowing to calculate an activation energy of dehydrogenation from the slope of the straight lines. The activation energies are summarized in Table 2 together with several values reported in the current literature for the MgH_2-doped systems. [26, 44, 47-57]

Additive	***E_a (kJ/mol)***
$VNbO_5$	**99**
MgH_2 milled 10h	115
Pure MgH_2[47]	174
$FeCl_3$[48]	130
V[49]	119
TiH_2[47]	131
Mg_2Ni[47]	98
C+Nb_2O_5[26]	102
Ni+rGO[50]	108
Cr_2O_3[51]	86
$MnFe_2O_4$[44, 58]	65, 108
Ni[52]	75

$BiVO_4$[34]	84
Co_2NiO[53]	118
TiO_2[54]	111
CeO_2[55]	109
$SrFe_{12}O_{19}$[56]	114
Ti[57]	37

Table 2. Energies Actions (Ea) values (kJ/mol) of several MgH_2-doped systems.

It should be noted that the $VNbO_5$-doped system showed a lower activation energy with respect to the un-doped system (99 vs 115 kJ/mol), proving that its faster hydrogen desorption kinetics was strictly correlated with the action of the dopant. Furthermore, the value extrapolated for the $VNbO_5$-doped system was similar,[47] and in most of case significantly lower[26, 48-50, 53-56] if compared with those of the most promising additives reported in the recent literature. As for the kinetics rate, the system milled with the ternary oxide $VNbO_5$ reported a higher destabilization than V-[49] and Nb_2O_5-catalyzed[26] systems. On the other hand, Ti-doped sample, investigated by Zhu and co-authors,[57] exhibited an extraordinary lower activation energy of 31 kJ/mol H_2 if compared with the $VNbO_5$-doped system here reported. However, in the former case, the catalyst was introduced by coating technique instead of mechanical treatment, with the disadvantage to supply solvent reagents and increase the cost of production. A lower value of activation energy (65 kJ/mol H_2), although no comparable with the previous case, was obtained by Li et al., when $MnFe_2O_4$ was added to MgH_2.[44] This very interesting value was not confirmed by a recent work published by Ismail and co-authors (108), despite the clear benefit, in terms of sorption kinetic, achieved introducing this ternary oxide.[58]

Considering the weighting impact of $VNbO_5$ on the hydrogen sorption kinetics of MgH_2, it was also relevant to investigate the relative thermodynamic stability of the 15 wt.-doped system. For this specific purpose, PCI curves (Figure 10) were acquired on the doped compound at 275 °C, 300 °C and 325 °C for the desorption (panel **a**) and absorption (panel **b**) steps.

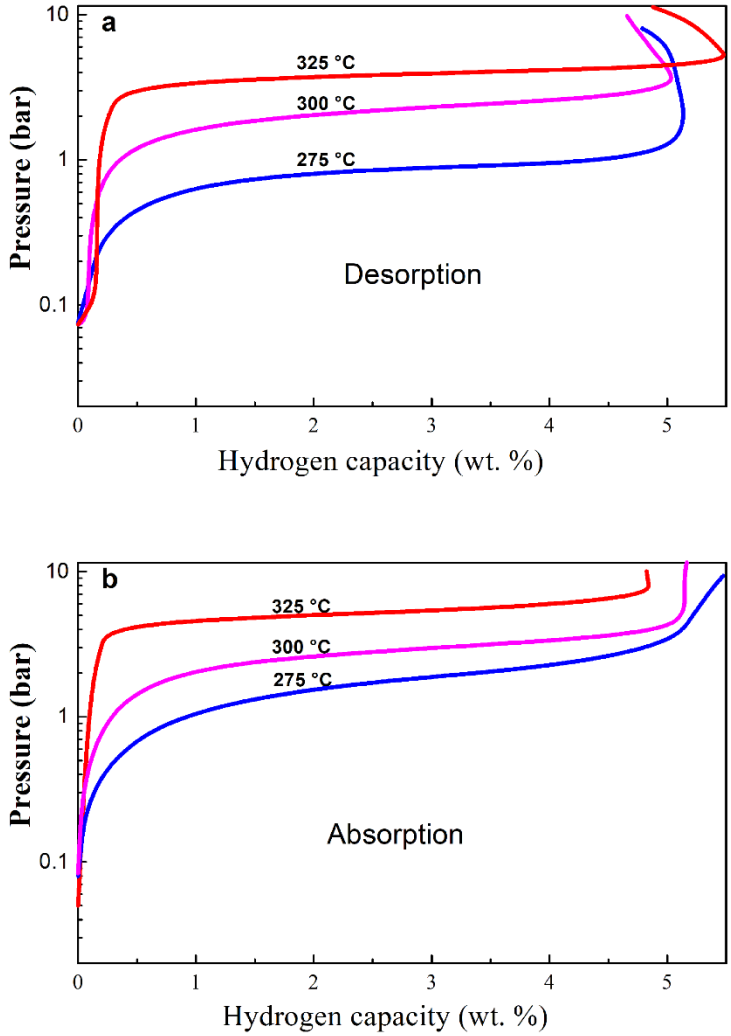

Figure 10. PCI desorption (a) and absorption (b) curves of MgH_2-15wt.%$VNbO_5$ determined at different temperatures.

PCI curves were characterized by a singular plateau pressure, confirming the equilibrium reaction (1):

$$MgH_2\ (cat) \leftrightarrow Mg\ (cat) + H_2 \quad (1)$$

Any other structural event related to the formation of MgV or MgNb could be then excluded suggesting, again, the stability of the catalyst.

For all the temperatures analysed, roughly 5 wt.% of hydrogen was desorbed and absorbed, although the system measured at 275 °C showed the lower equilibrium pressures of 0.87 and 1.81 bar for the desorption and absorption curves, respectively. The total equilibrium pressure P_{eq} were calculated starting for the plateau pressure values extrapolated from the absorption and desorption profiles using the equation 2:[59]

$$P_{eq} = \sqrt{P_{des}P_{abs}}$$ eq. 2

The equilibrium pressure can be correlated to the enthalpy reaction by the Van't Hoff equation 3:

$$ln\frac{P_{eq}}{P_0} = \frac{\Delta G}{RT} = \frac{\Delta H}{RT} - \frac{\Delta S}{R}$$ eq. 3

From the intercept and slope of the ln P_{eq}/P_0 versus 1/T (Van't Hoff plot), the entropy and enthalpy values of MgH_2-15wt.%$VNbO_5$ were derived. As reported in Figure 11, the change of enthalpy and entropy of the reaction (1) was 70.65 ± 0.43 kJ/mol H_2 and 114.73 ± 0.75 J/K mol H_2, respectively.

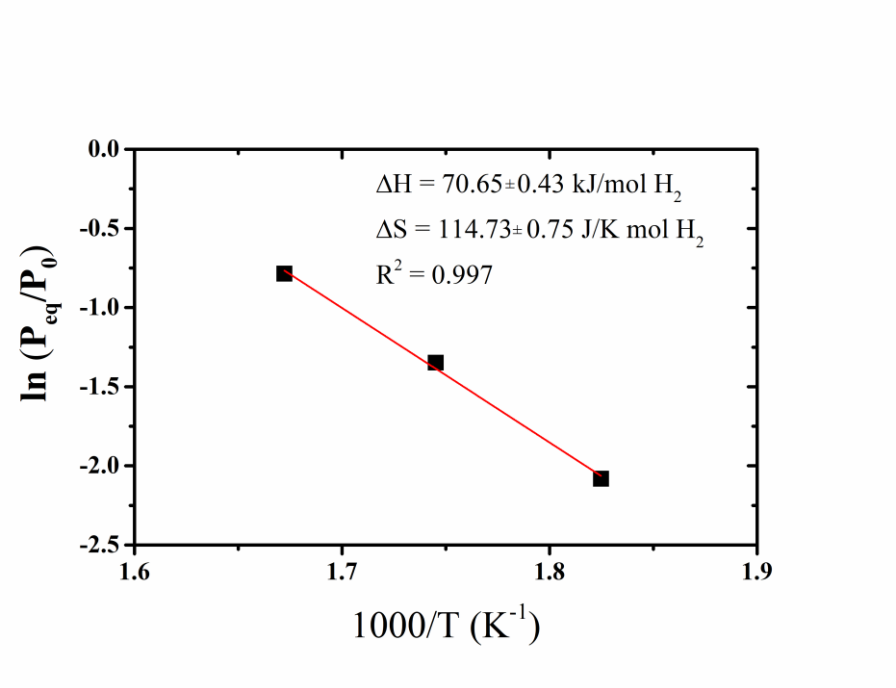

Figure 11. Van't Hoff plot for the MgH_2-15wt.% $VNbO_5$ system.

Comparing the enthalpy reaction value obtained with those of pure MgH_2 (77 kJ/mol H_2[60]) and according with other doped ZrF_4-[61] (75 kJ/mol H_2), NbF_5-[61] (77 kJ/mol H_2), TaF_5-[61] (75 kJ/mol H_2), $TiCl_3$-[61] (73 kJ/mol H_2), $SrTiO_3$-[62] (77 kJ/mol H_2) samples, it was possible to conclude that the addition of $VNbO_5$ apparently did not modify significantly the thermodynamic properties of MgH_2, but acted as an effective dopant with a clear reduction of the activation energy.

CONCLUSIONS

In this work, the catalytic effect of the as-synthesized $VNbO_5$ on the sorption properties of MgH_2 was, for the first time, experimentally investigated in detail. The addition of the catalyst, added in different concentrations (5, 10 and 15 wt.%), allowed to reduce the desorption temperature of MgH_2 down to 280 °C, which could be further decreased to 220 °C after the first hydrogenation cycle. Among the doped systems, the best performing composite was the 15wt. %-doped, which showed a total absorption of 5.5 wt. % of hydrogen in 10 minutes at 160 °C under 20 bar of hydrogen, and a full reversibility achieved at temperature of 275 °C for more than 50 cycles. Structural and microstructural characterizations were performed by X-ray diffraction on the ab-dehydrogenated powders. The analysis of the pattern profiles, performed by Rietveld refinement, proved the good dispersion of the catalyst in the whole system and any formation of secondary undesired phase. In order to quantify the kinetic barrier and thermodynamic stability of the catalysed-powders, the activation energy and the reaction enthalpy have been experimentally derived. The activation energy, E_a, calculated from the desorption process (99 kJ/mol), was significantly lower if compared to the 115 kJ/mol values obtained in the un-doped sample. Comparing with many dopants such as $FeCl_3$ (112 kJ/mol), V (119 kJ/mol), TiH_2 (131 kJ/mol), Nb_2O_5 (102 kJ/mol) and Ni+rGO (108 kJ/mol), the $VNbO_5$ showed a superior catalytic activity to destabilize the decomposition of MgH_2. Regarding the thermodynamic stability, the doped system reported a reaction enthalpy of ~ 71 kJ/mol H_2 similar to that obtained for the pure MgH_2. This value together with the linear equilibrium plateau achieved for the PCI curves collected at three different temperatures, confirmed that $VNbO_5$ plays a crucial role in the kinetic destabilization of the MgH_2 system.

From the findings reported in this manuscript it emerged that although the working temperature of 275 °C was significantly lowered with respect to the pure MgH_2 (400 °C), it is still too high for PEM Fuell cell powdered vehicles. However, the very fast kinetics rate achieved, among the best in the current literature, and the high number of cycles sustained, is leading this system to be a very promising candidate for off-board applications such as grid energy storage.

AKNOWLEGMENTS

This work was supported by the University of Sassari and MIUR (Italian Ministry for University and Research).

NOTES AND REFERENCES

1 T. R. Karl, J. M. Melillo and T. C. Peterson, *Global Climate Change Impacts in the United States*, Cambridge University Press, 2009.

2 S. Moroz, X. F. Tan, J. Pierce, M. Greaves, A. Duguid, K. Dumur and J. Ng, *J. Alloys Compd.* 2013**, 580**, S329-S332.

3 DOE, *Target Explanation Document: Onboard Hydrogen Storage for Light-Duty Fuel Cell Vehicles*, 2015, **7**.

4 J. C. Crivello, R. V. Denys, M. Dornheim, M. Felderhoff, D. M. Grant, J. Huot, T. R. Jensen, P. de Jongh, M. Latroche, G. S. Walker,C. J. Webb and V. A. Yartys,. *Appl. Phys. A*, 2016, **122**, 2.

5 I. Dovgaliuk and Y. Filinchuk, *Int. J. Hydrogen Energy*, 2016**, 41**, 15489-15504.

6 H. T Hwang and A. Varma, *Curr. Opin. Chem. Eng,*. 2014, **5**, 42-48.

7 C. Pistidda, N. Bergemann, J. Wurr, A. Rzeszutek, K. T. Møller, B. R. S. Hansen, S. Garroni, C. Horstmann, C. Milanese, A. Girella, O. Metz, K. Taube, T. R. Jensen, D. Thomas, H. P. Liermann, T. Klassen and M. Dornheim, *J Power Sources*, 2014**, 270**, 554-563.

8 O. Friedrichs, J. C. Sánchez-López, C. López-Cartes, M. Dornheim, T. Klassen, R. Bormann and A. Fernández, *Appl. Surf. Sci.*, 2006, **252**, 2334-2345.

9 N. Takeichi, K. Tanaka, H. Tanaka, T. T. Ueda, Y. Kamiya, M. Tsukahara, H. Miyamura and S. Kikuchi, *J. Alloys Compd.*, 2007**, 446**–**447**, 543-548.

10 S. Garroni, C. Pistidda, M. Brunelli, G. B. M. Vaughan, S. Suriñach and M. D. Baró, *Scripta Mater.*, 2009**, 60**, 1129-1132.

11 S. Garroni, C. Milanese, A. Girella, A. Marini, G. Mulas, E. Menéndez, C. Pistidda, M. Dornheim, S. Suriñach and M. D. Baró, *Int. J. Hydrogen Energy*, 2010, **35**, 5434-5441.

12 C. Pistidda, S. Garroni, C. B. Minella, F. Dolci, T. R. Jensen, P. Nolis, U. Bösenberg, Y. Cerenius, W. Lohstroh, M. Fichtner, M. D. Baró, R. Bormann and M. Dornheim, *J. Phys. Chem. C*, 2010, **114**, 21816-21823.

13 C. B. Minella, S. Garroni, C. Pistidda, G. Barkhordarian, C. Rongeat, I. Lindemann, O. Gutfleisch, T. R. Jensen, Y. Cerenius, I. Christensen, M. D. Baró, R. Bormann, T. Klassen and M. Dornheim, *J. Phys. Chem. C*, 2011, **115**, 2497-2504.

14 C. Milanese, S. Garroni, A. Girella, G. Mulas, V. Berbenni, G. Bruni, S. Suriñach, M. D. Baró and A. Marini, *J. Phys. Chem. C*, 2011, **115**, 3151-3162.

15 B. Zahiri, M. Danaie, X. Tan, B. S. Amirkhiz, G. A. Botton and D. Mitlin, *J. Phys. Chem. C* 2012, **116**, 3188-3199.

16 C. Milanese, A. Girella, S. Garroni, G. Bruni, V. Berbenni, P. Matteazzi and A. Marini, *Int. J. Hydrogen Energy*, 2010**, 35**, 1285-1295.

17 C. Ren, Z. Z. Fang, C. Zhou, J. Lu, Y. Ren and X. Zhang, *J. Phys. Chem. C*, 2014**, 118**, 21778-21784.

18 F. Cova, F. Gennari and P Arneodo Larochette, *Int. J. Hydrogen Energy*, 2014, **39**, 11501-11508.

19 S. Deledda, A. Borissova, C. Poinsignon, W. J. Botta, M. Dornheim and T. Klassen, *J. Alloys Compd.*, 2005**, 404–406**, 409-412.

20 S. A. Jin, J. H. Shim, J. P. Ahn, Y. W. Cho and K. W. Yi, *Acta Mater.*, 2007**, 55**, 5073-5079.

21 Y. Luo, P. Wang, L. P. Ma and H. M. Cheng, *J. Alloys Compd.*, 2008**, 453**, 138-142.

22 G. Barkhordarian, T. Klassen and R. Bormann, *Scripta Mater.*, 2003**, 49**, 213-217.

23 G. Barkhordarian, T. Klassen and R. Bormann, *J. Alloys Compd.*, 2004**, 364**, 242-246.

24 O. Friedrichs, T. Klassen, J. C. Sánchez-López, R. Bormann and A. Fernández, *Scripta Mater.*, 2006, **54**, 1293-1297.

25 A. Patah, A. Takasaki and J. S. Szmyd, *Int. J. Hydrogen Energy*, 2009**, 34**, 3032-3037.

26 C. Milanese, A. Girella, S. Garroni, G. Bruni, V. Berbenni, P. Matteazzi and A. Marini, *Int. J. Hydrogen Energy*, 2010**, 35**, 9027-9037.

27 H. G. Schimmel, J. Huot, L. C. Chapon, F. D. Tichelaar and F. M. Mulder, *J. Am. Chem. Soc.*, 2005**, 127**, 14348-14354.

28 O. Friedrichs, F. Aguey-Zinsou, J. R. A. Fernández, J. C. Sánchez-López, A. Justo, T. Klassen, R. Bormann and A. Fernández, *Acta Mater.*, 2006**, 54,** 105-110.

29 O. Friedrichs, J. C. Sánchez-López, C. López-Cartes, T. Klassen, R. Bormann and A. Fernández. *J. Phys. Chem. B* 2006, **110**, 7845-7850.

30 O. Friedrichs, D. Martínez-Martínez, G. Guilera, J. C. S. López and A. Fernández, *J. Phys. Chem. C*, 2007**, 111**, 10700-10706.

31 F. Dolci, M. Baricco, P. P. Edwards and E. Giamello, *Int. J. Hydrogen Energy*, 2008, **33**, 3085-3090.

32 W. Oelerich, T. Klassen and R. Bormann, *J. Alloys Compd.*, 2001, **322**, L5-L9.

33 D. Korablov, T. K. Nielsen, F. Besenbacher and T. R. Jensen, *Powder Diffr.*, 2015, **30**, S9-S15.

34 G. Xu, N. Shen, L. Chen, Y. Chen, W. Zhang, *Mater Res Bull*, 2017, **89**, 197-203.

35 Z. C. Wang, J. W. Liu, M. Schlangen, T. Weiske, D. Schroder, J. Sauer and H. Schwarz, *Chem. Eur. J.*, 2013, **19**, 11496-501

36 P. Tabero, E. Filipek and M. Piz, *Open Chemistry*, 2009, **7**, 222-227.

37 C. Börrnert, W. Carrillo-Cabrera, P. Simon and H. Langbein, *J. Solid State Chem.*, 2010, **183**, 1038-1045.

38 H. Langbein and T. Mayer-Uhma, *Mater. Res. Bull.*, 2009, **44**, 654-659.

39 P. Scardi, L. Lutterotti and P. Maistrelli, *Powder Diffr.* 1994, **9**, 180–186.

40 A. Motavalli, M. Rajabi and A. Gholipoor, *J. Adv. Mater. Proc.*, 2014, **2**, 67-72.

41 J. Zhang, J. Shan, P. Li, F Zhai, Q. Wan, Z. Liu and X. Qu, *J. Alloys Compd.*, 2015, **643**, 174-180.

42 R. A. Varin, T. Czujko, E. B. Wasmund and Z. S. Wronski, *J. Alloys Compd.*, 2007, **432**, 217-231.

43 M. Song, J. L. Bobet and B. Darriet, *J. Alloys Compd.*, 2002, **340,** 256-262.

44 P. Li, Q. Wan, Z. Li, F. Zhai, Y. Li, L. Cui, X. Qu and A. A. Volinsky, *J Power Sources*, 2013, **239**, 201-206.

45 P. A. Huhn, M. Dornheim, T. Klassen and R. Bormann, *J. Alloys Compd.*, 2005, **404–406**, 499-502.

46 H. E. Kissinger, *Anal. Chem.*, 1957, **432**, 1702-1706.

47 S. T. Sabitu, O. Fagbami and A. Goudy, *J. Alloys Compd.*, 2011, **509**, S588-S591.

48 M. Ismail, *Int. J. Hydrogen Energy*, 2014, **39**, 2567-2574.

49 T. Liu, T. Zhang, C. Qin, M. Zhu nd X. Li, *J Power Sources*, 2011, **196**, 9599-9604.

50 G. Liu, Y. Wang, F. Qiu, L. Li, L. Jiao and H. Yuan, *J. Mater. Chem.*, 2012, **22**, 22542.

51 M. Polanski and J. Bystrzycki, *J. Alloys Compd.*, 2009, **486,** 697-701.

52 M. S. El-Eskandarany, E. Shaban, N. Ali, F. Aldakheel and A. Alkandary, *Scientific Reports*, 2016, **6**, 37335.

53 N. Juanhir, N.S. Mustafa, A.M. Sinin, M. Ismail, *RSC Adv.*, 2015, **5**, 60983-60989.

54 D. Pukazhselvan, N. Nasani, P. Correia, E. Carbo-Argibay, G. Otero-Irurueta, D.G. Stroppa, D.P. Fagg, *J. Power Sources*, 2017, **362**, 174-183.

55 N.S. Mustafa, M. Ismail, *J. Alloy Compd*, 2017, **695**, 2532-2538.

56 N.S. Mustafa, N.N. Sulaiman, M. Ismail, *RSC Adv.*, 2016, **6**, 110004-110010.

57 J. Cui, H. Wang, J. Liu, L. Ouyang, Q. Zhang, D. Sun, X. Yao, M. Zhu, *J. Mater. Chem. A*, 2013, **1**, 5603-5611.

58 N.H. Idris, N.S. Mustafa, M. Ismail, *Int. J. Hydrogen Energy*, 2017, **42**, 21114-211120.

59 N. Patelli, M. Calizzi, A. Migliori, V. Morandi and L. Pasquini, *J. Phys. Chem. C*, 2017, **121**, 11166-11177.

60 J. J. Reilly and R. H. Wiswall, *Inorg. Chem.*, 1968, **7**, 2254-2256.

61 I.E. Malka, M. Pisarek, T. Czujko, J. Bystrzycki, *Int. J. Hydrogen Energy*, 2011, **36**, I2909-I2917.

62 M.S. Yahya, M. Ismail, *J Energy Chem*, 2017, in press, DOI: 10.1016/j.jechem.2017.10.020.